PHYSICAL REVIEW B **68**, 100406(R) (2003)

Spin-orbital phase diagram of perovskite-type $R\mathrm{VO_3}$ (R=rare-earth ion or Y)

S. Miyasaka,[1] Y. Okimoto,[2] M. Iwama,[1] and Y. Tokura[1,2,3]
[1]*Department of Applied Physics, University of Tokyo, Tokyo 113-8656, Japan*
[2]*Correlated Electron Research Center (CERC), National Institute of Advanced Industrial Science and Technology (AIST), Tsukuba 305-8562, Japan*
[3]*Spin Superstructure Project (SSS), ERATO, Japan Science and Technology Corporation (JST), Tsukuba 305-8562, Japan*
(Received 2 May 2003; published 23 September 2003)

The global phase diagram for the spin and orbital ordering has been investigated for perovskite-type $R\mathrm{VO_3}$ (R being a rare-earth ion or Y) by measurements of specific heat, magnetization, and Raman-scattering spectra. $R\mathrm{VO_3}$ (R=Lu-Pr), in which the large tilting of $\mathrm{VO_6}$ tends to stabilize the collective Jahn-Teller distortion, shows a structural phase transition concomitantly with the G-type orbital ordering (OO) at a temperature far above the C-type magnetic transition temperature. By contrast the C-type spin correlation appears to develop primarily and then induce the G-type OO in $\mathrm{CeVO_3}$ and $\mathrm{LaVO_3}$ with smaller lattice distortion.

DOI: 10.1103/PhysRevB.68.100406 PACS number(s): 75.30.Kz, 71.27.+a, 71.30.+h

In transition-metal oxides, strong electron correlation plays an important role in producing a variety of intriguing physical properties, such as Mott transition, high-T_c superconductivity, and colossal magnetoresistance (CMR).[1,2] Recent investigations on the CMR manganese oxides have raised great interest in the interplay among spin, charge, orbital, and lattice degrees of freedom, particularly in the orbital ordering (OO) and related phenomena.[3,4] As well as the manganites, vanadium oxides have been regarded as one of the most prototypical systems that show spin-charge-orbital coupled phenomena. In the V^{3+}- or V^{4+}-based oxides where only the t_{2g} orbital electrons are active, the Jahn-Teller interaction is weaker than that in manganese oxides with partially filled e_g orbitals. As a result, the OO in such a t_{2g} orbital system becomes relatively amenable to thermal agitation and hence the relationship among spin, orbital, and lattice degrees of freedom is even more subtle and complex than that in the e_g orbital one. To investigate the lattice effect on the spin and orbital states in the t_{2g} orbital system, we have revisited classic Mott insulators, perovskite-type $R\mathrm{VO_3}$ with R being a trivalent rare-earth ion or Y.

Perovskite-type $R\mathrm{VO_3}$ has a $Pbnm$ orthorhombic lattice with the lattice constants of $a \approx b \approx c/\sqrt{2}$ at room temperature, and exhibits two kinds of spin-ordered state depending on the R-site ions.[5–7] Those spin-ordering (SO) patterns are shown in the insets of Fig. 1. When the R-site ionic radius is large and hence the orthorhombic lattice distortion is small, the antiferromagnetic (AF) structure at low temperatures is C-type with the ferromagnetically arranged V^{3+} ($S=1$) spins along the c-axis and the antiferromagnetically coupled ones in the ab plane. One such compound showing this SO is $\mathrm{LaVO_3}$. In $R\mathrm{VO_3}$ with relatively small R-site ions, on the other hand, the pattern of the SO at the ground state is G-type with an AF coupling between V^{3+} ($S=1$) spins in all three directions. $\mathrm{YVO_3}$, which shows a temperature (T)-induced magnetization reversal phenomenon,[8] is located near the boundary between the C-type and G-type AF phases, and undergoes the magnetic transition from C-type to G-type with decreasing T.[6,7]

Among the perovskite-type $R\mathrm{VO_3}$, the OO phenomenon has been investigated so far for $\mathrm{YVO_3}$ and $\mathrm{LaVO_3}$. These compounds undergo structural phase transitions accompanied by the ordering of the t_{2g} orbital as T is decreased. The patterns of the OO in both the compounds are schematically drawn in the insets of Fig. 1. In $\mathrm{YVO_3}$, a resonant x-ray scattering study as well as a single-crystal x-ray diffraction measurement has confirmed the existence of two types of

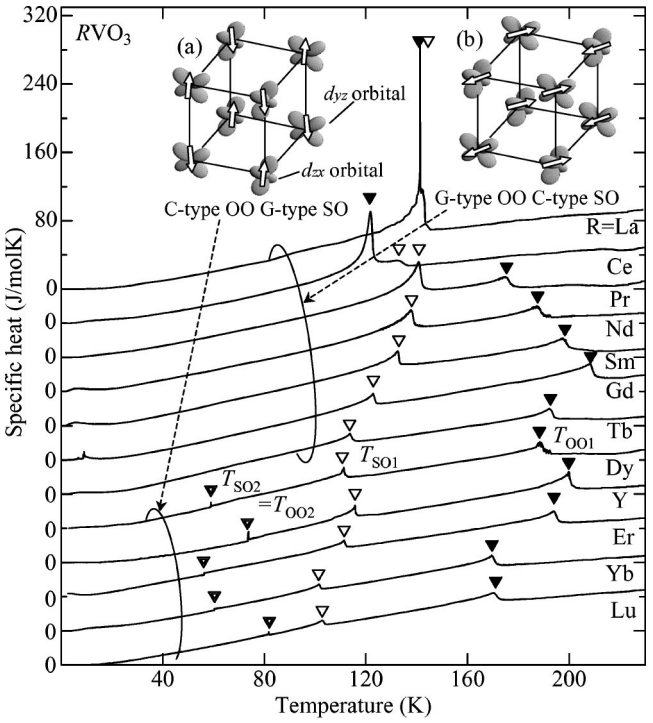

FIG. 1. Temperature dependence of specific-heat for $R\mathrm{VO_3}$ (R=La-Lu). The closed, open, and double triangles indicate the transition temperatures of the G-type orbital ordering (T_{OO1}), C-type spin ordering (T_{SO1}), and G-type spin and C-type orbital ordering ($T_{SO2}=T_{OO2}$), respectively. The insets, (a) and (b), show the structures of the C-type orbital ordering (OO) and G-type spin ordering (SO), and the G-type OO and C-type SO in $R\mathrm{VO_3}$, respectively. Open arrows and lobes indicate spins, and occupied d_{yz} and d_{zx} orbitals on the vanadium ions, respectively. The commonly occupied d_{xy} orbitals are displaced for clarity.

orbital-ordered states.[9,10] In this compound, the structural phase transition from an orthorhombic to a monoclinic form takes place concomitantly with the OO at 200 K, which is far above the *C*-type magnetic transition T ($T_{SO1}=115$ K). In this orbital-ordered phase, YVO_3 has the commonly occupied d_{xy} orbital and alternately occupied d_{yz} or d_{zx} one. Here, we call this the *G-type* OO by analogy to SO. Below the *G*-type SO transition T ($T_{SO2}=71$ K), where a distortion of an octahedral VO_6 changes due to the collective Jahn-Teller effect,[6] the pattern of the OO turns into *C*-type with the alternate $d^1_{xy}d^1_{yz}/d^1_{xy}d^1_{zx}$ electron configuration in the ab plane and the identical one along the *c*-axis. In contrast with YVO_3, $LaVO_3$ undergoes the structural phase transition at only a few degrees below $T_{SO1}=143$ K with the decrease of T.[11,12] Sawada *et al.* showed by the generalized gradient approximation calculation that the *G*-type OO should be present in the lower-T monoclinic phase.[13] The investigation of optical spectra has provided a further evidence for the existence of the *G*-type OO below the structural phase transition T in this compound.[14–16]

Thus, the SO and OO phenomena are quite different between $LaVO_3$ and YVO_3, not only the ground-state patterns but also the T-dependent sequential order of the OO and SO transitions. Such a difference between both the compounds may arise from the different magnitude of the tilting of VO_6 octahedra in distorted perovskite lattice. The V-O-V bond angles are 144.8° and 144.3° for $R=$Y, while 157.8° and 156.7° for $R=$La.[6,12] To interpolate these possibly extreme cases as well as to obtain a broader perspective of the lattice effect on the OO and SO, we have investigated systematically specific heat, magnetization, and Raman-scattering spectra for $R\mathrm{VO}_3$ with R ranging from Lu to La (plus Y) by using high-quality single crystals. Thus, the global phase diagram of the SO and OO and the interplay between the orbital and the AF spin have been clarified.

All the samples of $R\mathrm{VO}_3$ used in the present studies are single crystals grown by a floating-zone method according to the procedure described elsewhere.[11] Specific-heat measurements were performed by a relaxation method. Magnetization measurements were carried out with a superconducting quantum interference device magnetometer. In the measurements of the Raman-scattering spectra, we used the $(a+b)c$ plane of the crystals. The spectra presented here were measured in a polarization configuration of (xx), where the notation of x represents the polarization of incident or scattering light along the $(a+b)$ axis. A 632.8 nm light from a He-Ne laser (3 mW) was focused onto a 0.05-mm-diameter spot on the sample surface.

We display the T dependence of the specific heat for the crystals with varying *R*-site ions in Fig. 1. All the specific-heat curves have two or three peaks due to the magnetic transitions and/or the structural ones coupled with the OO.[17] These phase-transition temperatures for the respective compounds are summarized in Fig. 2 as the spin-orbital phase diagram. (Account for the phase diagram is given later.) For example, the specific-heat curve in YVO_3 (Fig. 1) shows three jumps. Those correspond to the structural phase transition occurring concomitantly with the *G*-type OO at 200 K, the *C*-type AF transition at 115 K, and the transition to the

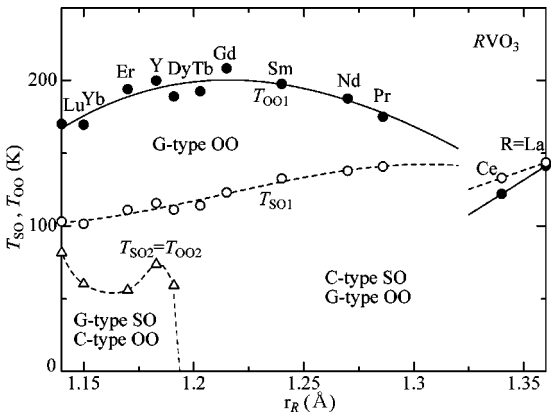

FIG. 2. Spin-orbital phase diagram of $R\mathrm{VO}_3$ ($R=$Lu-La) over an entire region of the *R*-site ionic radius r_R. Closed and open circles, and open triangle indicate the transition temperatures of the *G*-type orbital ordering (OO) (T_{OO1}), the *C*-type spin ordering (SO) (T_{SO1}), and the *G*-type SO and *C*-type OO ($T_{SO2}=T_{OO2}$), respectively.

G-type spin- and *C*-type orbital-ordered state at 71 K, respectively. The specific-heat measurements have revealed that the compound with a small *R*-site ion ($R=$Lu to Dy) undergoes such successive three-phase transitions with the decrease of T. The result of the magnetization indicates that the two transitions occurring below 120 K are due to the AF SO. Therefore it is likely that $R\mathrm{VO}_3$ ($R=$Lu-Dy) has the similar sequence of spin- and orbital-ordered phases as YVO_3, i.e., the higher-T *G*-type orbital-ordered paramagnetic phase, the intermediate-T *G*-type orbital- and *C*-type spin-ordered one, and the lower-T *C*-type orbital- and *G*-type spin-ordered one.

In the compounds with an intermediate size of R (=Tb to Pr), the specific-heat shows an anomaly around 130 K (indicated by open triangles), which is caused by the *C*-type AF transition.[5] Besides this magnetic transition at T_{SO1}, another transition indicated by closed triangles takes place at $T=T_{OO1}$ above T_{SO1} in these materials. This highest-lying transition is ascribed to the structural phase change associated with the *G*-type OO, as also evidenced by the following arguments (Figs. 3 and 4). Both transition temperatures show a systematic change when the R site is changed from Tb to Pr. In contrast with $R\mathrm{VO}_3$ with $R=$Tb-Pr, $CeVO_3$ and $LaVO_3$ with a relatively large R ion undergo this structural phase transition right below T_{SO1}. This was unambiguously concluded by comparison between the specific-heat and magnetization data. For example, the specific-heat peak that is accompanied with the magnetization change is the higher-lying one in $CeVO_3$, while that is the lower-lying one in $PrVO_3$, as indicated by open triangles in Fig. 1. In $LaVO_3$, the investigation of the x-ray diffraction has already confirmed that this transition is due to the structural change from the orthorhombic to the monoclinic form.[12] The result of the specific heat as compared with the T-dependent magnetization indicates that not only $LaVO_3$ but also $CeVO_3$ undergoes the similar structural phase transition coupled with the *G*-type OO at only 2–8 K below T_{SO1}.

Raman-scattering spectroscopy can be used as a probe for the OO because of its sensitivity to lattice distortion induced

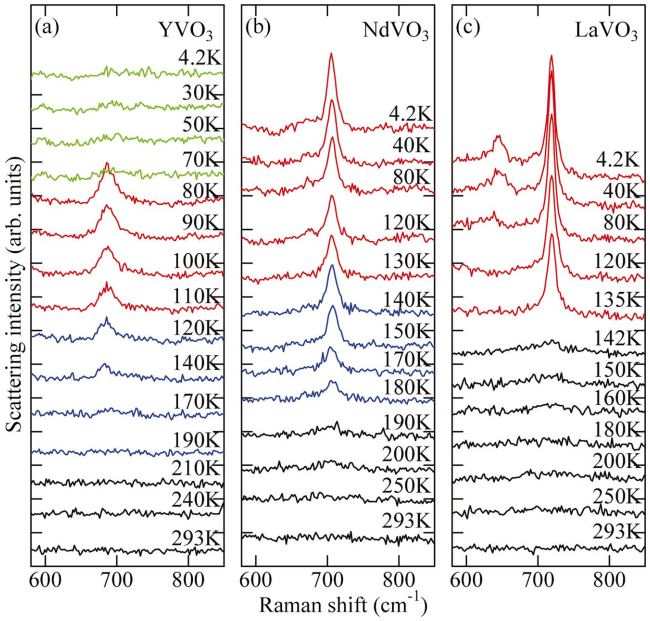

FIG. 3. (Color) Phonon (oxygen stretching mode) Raman spectra for the polarization configuration of (xx) at various temperatures in single crystals of (a) YVO_3, (b) $NdVO_3$, and (c) $LaVO_3$. Black, blue, red, and green lines show the spectra in the paramagnetic phase, the *G*-type orbital-ordered one, the *C*-type spin- and *G*-type orbital-ordered one, and the *G*-type spin- and *C*-type orbital-ordered one, respectively.

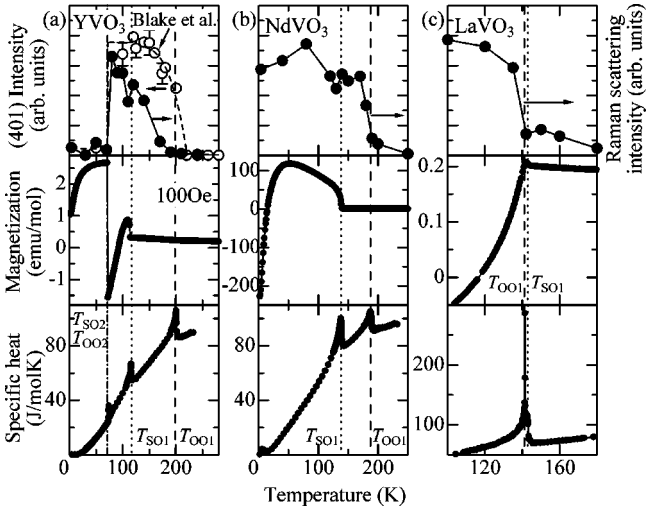

FIG. 4. Temperature dependence of the integrated Raman-scattering intensity of the peak around 700 cm^{-1} (upper panel), magnetization (middle panel), and specific heat (bottom panel) for (a) YVO_3, (b) $NdVO_3$, and (c) $LaVO_3$. The temperature dependence of the intensity of the x-ray (401) reflection reported by Blake *et al.*[10] is also shown in the top panel of (a). Vertical broken, dotted, and dash-dotted lines indicate the transition temperatures of the *G*-type orbital ordering (T_{OO1}), the *C*-type spin ordering (T_{SO1}), and the *G*-type spin and *C*-type orbital ordering ($T_{SO2}=T_{OO2}$), respectively.

by the collective Jahn-Teller coupling.[18] Figure 3 presents the Raman spectra of the oxygen stretching modes in the polarization configuration of (xx) for YVO_3, $NdVO_3$, and $LaVO_3$ at various temperatures.[19] In the spectra for YVO_3, a peak-structure is observed at 687 cm^{-1} only between the first and second structural phase transition temperatures $[T_{OO1}=200\ \mathrm{K}>T>T_{OO2}=71\ \mathrm{K}\ (=T_{SO2})]$. As well as the 687 cm^{-1} peak for YVO_3, a sharp peak in the Raman spectra for $NdVO_3$ and $LaVO_3$ appears at 705 and 719 cm^{-1}, respectively, only in a low-T region. The Raman shifts of these peak structures are close to each other and show a slight but systematic increase with the increase of the *R*-site ionic radius. This behavior suggests that these bands around 700 cm^{-1} in the Raman spectra for RVO_3 (R=Y, Nd, and La) share the same origin.

For YVO_3, Blake *et al.* have observed the x-ray (401) diffraction only between T_{OO1} and T_{OO2},[10] where the 687 cm^{-1} peak appears in the Raman spectrum. We plot the *T*-dependent intensity of the x-ray (401) reflection[10] and the integrated one of the 687 cm^{-1} Raman peak in the top panel of Fig. 4(a). The existence of the reflection (401) suggests that the $Pbnm$ symmetry is violated and that the structure turns into the $P2_1/a$ monoclinic form in the T region of $T_{OO2}<T<T_{OO1}$ in YVO_3. Thus, the 687 cm^{-1} Raman band in YVO_3 is activated only in the monoclinic $P2_1/a$ phase coupled with the *G*-type OO. Below T_{OO2}, both the reflection (401) and the 687-cm^{-1} Raman peak disappear. These behaviors show that the monoclinic structure turns into the lower-T orthorhombic one below T_{OO2}, where the pattern of the OO changes into *C*-type. The middle and bottom panels in Fig. 4(a) clearly show that the anomalies of the specific heat are caused not only by the AF transition at T_{SO1}, which is manifested by the magnetization behavior, but also by these two structural ones at T_{OO1} and $T_{OO2}(=T_{SO2})$.[20]

In $NdVO_3$, the peak at 705 cm^{-1} in the Raman spectrum is distinctly observed below around 180 K, as seen in Figs. 3(b) and 4(b). The appearance of the 705 cm^{-1} band indicates via the analogy to the case of YVO_3 that the structure changes into the monoclinic form concomitantly with the *G*-type OO around 180 K in $NdVO_3$. Besides the structural phase transition, this compound undergoes the magnetic one to the *C*-type AF state at $T_{SO1}=138$ K, where both the specific heat and the magnetization show a jump. As seen in Fig. 1, the specific heat vs T curve shows a very similar behavior for RVO_3 with R ranging from Tb to Pr. Therefore it is obvious that not only $NdVO_3$ but also other RVO_3 with R =Tb-Sm or R=Pr undergo the structural phase transition accompanied by the *G*-type OO at a temperature $(=T_{OO1})$ far above T_{SO1}. As seen in Fig. 3(c), the sharp peak at 719 cm^{-1} in the spectrum for $LaVO_3$ is observed only in the $P2_1/a$ monoclinic phase, although it is difficult to distinguish the closely neighboring T_{OO1} and T_{SO1} by the Raman data alone. In the magnetization and specific-heat curves [Fig. 4(c)], the T_{OO1} is clearly discerned to position immediately below T_{SO1}. (Quite a similar relation between the magnetization and specific-heat curves is confirmed also for $CeVO_3$ with the same sequence of the spin- and orbital-ordering transitions.)

To overview the lattice effect on the interplay between spin and orbital degrees of freedom in RVO_3, the extended

phase diagram is shown in Fig. 2. The compounds with R = Lu to Pr undergo the orthorhombic-monoclinic structural phase transition concomitantly with the G-type OO at T_{OO1} that positions above T_{SO1}, indicating that the orbital correlation grows at high temperatures without long-range magnetic ordering. As the ionic size of the R-site is increased from Lu to La, the orthorhombic distortion, which shows the same tilting habit of VO_6 octahedra as the collective Jahn-Teller one coupled with the G-type OO, is gradually decreased. The decreasing V-O-V bond angle distortion may result in increase of transfer interaction and hence in enhancement of the spin and orbital exchange interactions between the nearest-neighbor V sites.[5,10,12] The T_{SO1} monotonously increases perhaps due to the increase of exchange interaction as the R site is changed from Lu to Pr. With the increase of the R-site ionic radius, on the other hand, T_{OO1} reaches the maximum around R = Gd and decreases towards R = Pr. This is perhaps a result of the competition between the increase of the orbital exchange interaction and the suppression of the Jahn-Teller instability. Finally, T_{OO1} and T_{SO1} cross at between R = Pr and Ce. In $CeVO_3$ and $LaVO_3$, the magnetic ordering takes place at first with the decrease of T, and subsequently the structural phase transition coupled with the OO occurs at a few degrees below T_{SO1}. The G-type OO transition T, T_{OO1}, does not decrease any more departing from T_{SO1}, when it locates below T_{SO1}, i.e., in the case of R = Ce and La. In other words, when the long-range C-type SO is established, it appears to immediately induce the G-type OO. A recent theoretical investigation of spin-orbital model for $LaVO_3$[15] has shown that the C-type long-range SO endows the orbital system (yz/zx orbitals) with the one-dimensional nature along the c-axis, which produces the strong Jahn-Teller lattice instability coupled with the G-type OO. This explains why the T_{OO1} always sticks to T_{SO1} when $T_{OO1} < T_{SO1}$, as observed. Incidentally, the feature that the G-type OO immediately follows the C-type SO (i.e., $T_{SO1} - T_{OO1} = 2-5$ K) is observed even in a hole-doped system $La_{1-x}Sr_xVO_3$ ($x < 0.178$),[11] suggesting that the C-type SO urges the G-type OO as well as in the parent ($x = 0$) compound. Thus, the sequential order and causality concerning the SO and OO are opposite between the compounds with R = Lu-Pr and with R = Ce and La. At the ground state, RVO_3 undergoes the transition from the C-type spin- and G-type orbital-ordered phase to the G-type spin- and C-type orbital-ordered one with the decrease of the R-site ionic radius or equivalently with the increase of the $GdFeO_3$-type orthorhombic distortion. The compounds with R = Lu to Dy show the T-induced change of the spin (orbital) ordering from the lower-T G-type (C-type) to the higher-T C-type (G-type).

In summary, the global spin-orbital phase diagram has been clarified for the perovskite RVO_3 with R = rare earth and Y on the basis of the experimental investigations of magnetization, specific heat, and Raman scattering on the single-crystalline compounds. The collective Jahn-Teller distortion coupled with the orbital ordering tends to be stabilized by the orthorhombic distortion ($GdFeO_3$-type distortion), while the spin/orbital exchange interactions appear to be decreased with the distortion. Thus, the lattice effect appears to play a crucial role in causing such a large variety of phase transitions and their thermal sequence with change of R species as demonstrated in Fig. 2.

We would like to thank H. Okamoto, Y. Motome, H. Seo, N. Nagaosa, T. Arima, and B. Keimer for helpful discussions. This work was supported in part by Grant-In-Aids for science research from the MEXT, Japan.

[1] N.F. Mott, *Metal-Insulator Transitions* (Taylor and Francis, London, 1990).
[2] For a review, see M. Imada, A. Fujimori, and Y. Tokura, Rev. Mod. Phys. **70**, 1039 (1998).
[3] For a review, see *Colossal Magnetoresistive Oxides*, edited by Y. Tokura (Gordon and Breach, New York, 2000).
[4] Y. Tokura and N. Nagaosa, Science **228**, 462 (2000).
[5] V.G. Zubkov *et al.*, Sov. Phys. Solid State **15**, 1079 (1973).
[6] H. Kawano *et al.*, J. Phys. Soc. Jpn. **63**, 2857 (1994).
[7] C. Ulrich *et al.*, cond-mat/0211589 (unpublished).
[8] Y. Ren *et al.*, Nature (London) **396**, 441 (1998); Y. Ren *et al.*, Phys. Rev. B **62**, 6577 (2000).
[9] M. Noguchi *et al.*, Phys. Rev. B **62**, 9271 (2000).
[10] G.R. Blake *et al.*, Phys. Rev. Lett. **87**, 245501 (2001).
[11] S. Miyasaka, T. Okuda, and Y. Tokura, Phys. Rev. Lett. **85**, 5388 (2000).
[12] P. Bordet *et al.*, J. Solid State Chem. **106**, 253 (1993).
[13] H. Sawada *et al.*, Phys. Rev. B **53**, 12 742 (1996).
[14] S. Miyasaka *et al.*, J. Phys. Soc. Jpn. **71**, 2086 (2002).
[15] Y. Motome *et al.*, Phys. Rev. Lett. **90**, 146602 (2003).
[16] Z. Fang, N. Nagaosa, and K. Terakura, Phys. Rev. B **67**, 035101 (2003).
[17] The anomalies in the specific heats below 20 K are due to the ordering of the R^{3+} moments.
[18] For example, K. Yamamoto *et al.*, Phys. Rev. B **61**, 14 706 (2000); E. Saitoh *et al.*, J. Phys. Soc. Jpn. **69**, 3614 (2000).
[19] We observed a systematic change not only for the oxygen stretching modes but also for the oxygen bending ones. The Raman shift of the oxygen bending mode changes from 352 to 305 cm^{-1}, as the R site is varied from Y to La, perhaps reflecting the change in V-O-V bond angles in the orthorhombic lattice form.
[20] Among RVO_3, several compounds (R = La, Nd, Gd, Sm, and Y) show the T-induced magnetization reversal phenomenon as reported in detail for R = Y (Ref. 8). However, each low-field magnetization and its T-dependent feature varies in a R-dependent manner.